ISSN 1068-3356, Bulletin of the Lebedev Physics Institute, 2023, Vol. 50, No. 8, pp. 318–331. © Allerton Press, Inc., 2023.

# Broadband Supercontinuum Generation with Low Peak Power in a Circular Lattice Nitrobenzene-Core Photonic Crystal Fiber

**D. V. Trong[a],* (ORCID: 0000-0001-5216-9308) and C. V. Lanh[a],** (ORCID: 0000-0001-7738-6720)**

[a] *Department of Physics, Vinh University, Vinh city 461010, Nghe An Province, Vietnam*

**e-mail: dangvantrong0602@gmail.com*

***e-mail: chuvanlanh@vinhuni.edu.vn*

Received April 11, 2023; revised June 27, 2023; accepted June 28, 2023

**Abstract**—We highlight the advantage of varying the filling factor $d_1/\Lambda$ in the first cladding ring of a nitrobenzene-core ($C_6H_5NO_2$-core) photonic crystal fiber (PCF) with a circular lattice in improving the fiber nonlinearity. Joint optimization of feature sets can be achieved to achieve flat dispersion, small effective mode area, and low loss while controlling structural parameters such as filling factor ($d_1/\Lambda$) and lattice constant ($\Lambda$). Two optimal PCFs were selected and studied in detail for broadband and low peak power supercontinuum generation. The first PCF with a lattice constant ($\Lambda$) of 1.0 μm and a filling factor of 0.65 has an all-normal dispersion in the wavelength range from 0.5 to 2.0 μm. When a 90 fs pulse centered at 1.3 μm is pumped into a 1 cm long fiber with a peak power of only 133 W, the supercontinuum spectrum produced extends from the visible to the near-infrared (0.72–1.722 μm) range. On the other hand, a second PCF with $\Lambda$ of 2.0 μm and $d_1/\Lambda$ of 0.3 has anomalous dispersion and has a zero dispersion wavelength at 1.547 μm. By using a 110 fs input pulse with a peak power of 273 W and a pump wavelength of 1.56 μm, broad SC generation with a spectral bandwidth of 0.795–3.748 μm was achieved for a 15 cm long sample. The proposed design could become a new class of microstructured optical fibers for the broadband supercontinuum generation.

**Keywords:** photonic crystal fiber (PCF), nitrobenzene-core ($C_6H_5NO_2$-core), circular lattice, supercontinuum generation, all-normal dispersion, anomalous dispersion

**DOI:** 10.3103/S1068335623080080

## INTRODUCTION

Supercontinuum generation (SCG) is a phenomenon that occurs when dispersion interacts with nonlinear effects in nonlinear media [1]. Fiber-based supercontinuum (SC) light sources are widely used in optical frequency measurement [1], ultrashort pulse generation [2], and telecommunications [3]. In recent years, photonic crystal fibers (PCFs) have become the most widely used objects in SCG processes due to their high nonlinearity and tunable dispersion properties. The generation of spectral continuum radiation is achieved by contributions of multiple linear and nonlinear optical effects and is closely related to the dispersive configuration exhibited by optical waveguides. Depending on the choice of pump wavelength within the dispersion range, corresponding effects occur in his SCG. In particular, the SC generated by pumping in the anomalous dispersion regime is achieved by contributions of soliton dynamics, dispersive waves, and Raman frequency shifts [4–6]. Although the pump wavelength is chosen in the normal dispersion range, self-phase modulation (SPM) and optical wave breaking (OWB) are effects that contribute to spectral broadening [7]. SCG performance depends on pump parameters such as input pulse energy, pulse duration, pump wavelength, fiber nonlinearity, and fiber length.

Considerable efforts have been made to extend the spectral width and improve the spectral flatness of SC sources. To achieve this, PCFs require a special design that achieves both flat dispersion and highly nonlinear properties, and should be optimized using pump wavelength and input power [8]. To achieve the best SCG efficiency, the PCF's chromatic dispersion curve should be flat and close to zero, and the attenuation and effective mode area should be as small as possible. Structural parameters of PCFs such as lattice constant, pore size, shape, solid or hollow core, and materials can be designed and tuned to achieve such goals.

Scientists have attempted to efficiently generate SC generation using highly nonlinear quartz or glass PCFs [9–11]. Silica is often used in SC generation due to its special purity and very high laser damage

threshold. However, fused silica is not transparent in the mid-infrared (m-IR) and exhibits relatively low nonlinearity. On the other hand, his PCF from highly nonlinear glasses can produce SC generation in the m-IR range. However, a drawback of using soft glass fibers for SGs is their incompatibility with silica-based fiber systems typically run in expensive and complex experimental systems [10, 11]. Recently, a promising alternative using liquid-filled hollow-core fibers with high nonlinear refractive index and high transparency was investigated for efficient SC generation. This leads to the emergence of interesting nonlinear phenomena, especially the generated SCs with lower peak powers than solid fibers [12]. It is now possible to introduce liquid into the air core by advanced methods [13–16]. In this way, several nonlinear liquids, named a few, carbon disulfide ($CS_2$) [17, 18], carbon tetrachloride ($CCl_4$) [19–21], chloroform ($CHCl_3$) [22], nitrobenzene ($C_6H_5NO_2$) [15], benzene ($C_6H_6$) [23], tetrachloroethylene ($C_2Cl_4$) [16, 24], 1-2 dibromoethane ($C_2H_4Br_2$) [25], and toluene ($C_7H_8$) [12, 26] have been used for this approach. The results showed that the generated SC spectra can be controlled by changing the temperature and pressure or by applying an electric field [27]. Also, SC spectra can be obtained with high coherence in both normal and anomalous dispersion regions [28]. However, his PCF in the above analysis has the same air hole size in the lattice cladding, so only the dispersion can be optimized, but not the effective area and loss. Although it cannot be denied that previous work has attempted to increase the SC bandwidth, such levels are still not ideal due to the limited spectral bandwidth due to the high input powers and long fiber lengths used.

In general, hexagonal lattices are more commonly used in the design of PCF structures, while circular lattices have been less studied. Circular lattice are more symmetrical, amplifying the light in the core better and improving the nonlinearity of the fiber. Recently, an SCG with a circular PCF lattice with toluene cores was reported [29]. In this work, the author highlights the difference between the diameter of the air hole of the first ring and the diameter of the remaining grid his rings, which helps to optimize the characteristic size. The SC spectrum in this work is obtained flat and smooth over a wide range of wavelengths. In particular, the spectral range obtained in the perfectly normal dispersion region is 0.642–1.592 μm with a peak power of 450 W, whereas in the anomalous dispersion region it is 0.911–2.496 μm with a peak power of 550 W. However, the performance regarding spectral flatness, bandwidth, and coherent SC spectrum needs further optimization.

In this article, we discuss the use of microstructured circular lattice PCFs with $C_6H_5NO_2$ core for SC generation. With the goal of generating a broadband coherent SC spectrum from the visible to the mid-IR at very low input power, the cross-section of the PCF is specifically designed to accommodate the different diameters of the air holes in the lattice rings. The lattice constant ($\Lambda$) and filling factor ($f_1$) are then appropriately controlled to optimize the linear and nonlinear optical parameters, resulting in a flat dispersion profile and near-zero dispersion wavelength, small effective mode area, and minimal attenuation to ensure. A series of numerical simulations are performed to investigate the effects of initial pulse characteristics (input peak power and pulse duration) on the SC bandwidths of the two optimal structures, achieving wider bandwidths than previous low-peak power work.

The article is structured as follows. Section 2 describes the proposed microstructured PCF with a liquid-filled core. Section 3 presents parameter optimization. The extended SC spectra are generated with optimized PCFs with lower peak power compared to previous work described in Section 4. This work concludes with the conclusions in Section 5.

## NUMERICAL MODELING

In this section, we design a photonic crystal fiber by using Lumerical Mode Solution software based on the finite-difference eigenmodes (FDE) [30]. The geometry of the circular lattice $C_6H_5NO_2$ core PCF is modeled as shown in Fig. 1. The simulation process uses perfectly matched layers with scattering boundary conditions. This allows the radiation to propagate outside the calculated domain even though the interferometer has no internal field or absorption limit for the incident light. Circular PCF structures were chosen for investigation because of their significant advantages over other gratings. The high symmetry enhances the supercontinuum generation efficiency by confining the light entering the core and increasing the nonlinearity. This means better bandwidth extension than other gratings. The base material is quartz glass ($SiO_2$), and the core is filled with $C_6H_5NO_2$ to increase the refractive index difference between the core and the clad, improving light confinement in the core. $C_6H_5NO_2$ enters the core by integrating a fusion splicer [26] or a microfluidic injection system using laser writing technology [31].

The high nonlinear refractive index, $n = 671 \times 10^{-20}$ m$^2$ W$^{-1}$ at 1064 nm [32], which is about 240 times higher than that of silica [33], emphasizes the choice of nitrobenzene for filling hollow-core PCFs, which

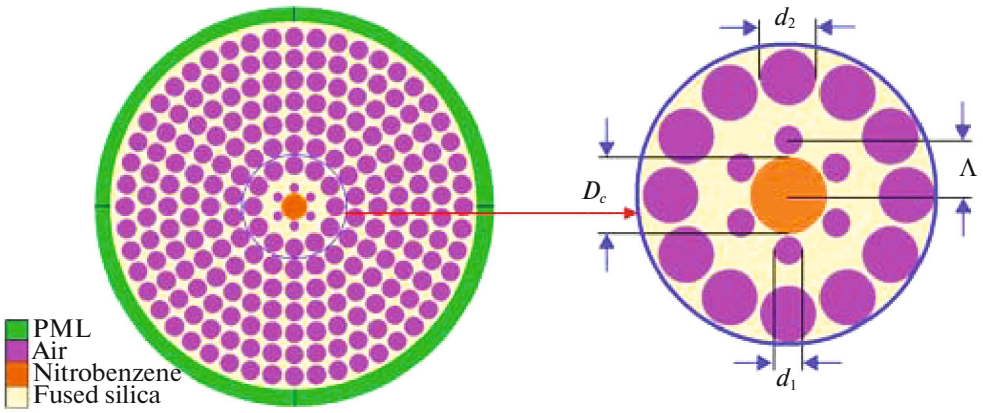


**Fig. 1.** Cross-section view of the circular $C_6H_5NO_2$-PCF.

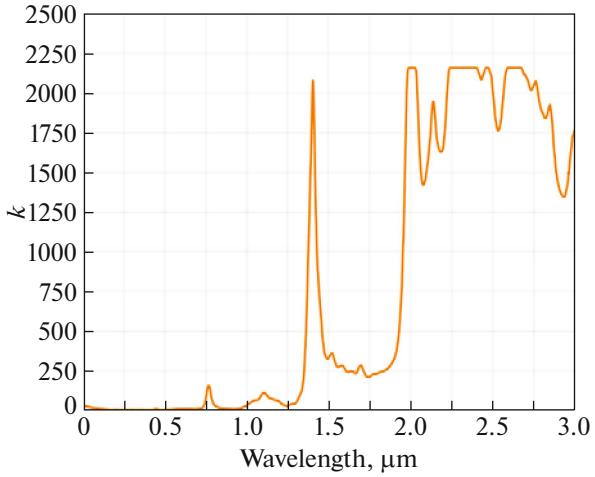


**Fig. 2.** The imaginary part of the refractive index $k$ of $C_6H_5NO_2$.

is higher than other liquids such as $CHCl_3$ [22], $CCl_4$ [19–21], $C_2Cl_4$ [16, 24], and $C_7H_8$ [26]. Nitrobenzene is a water-insoluble pale yellow oil with a specific almond odor. Figure 2 shows the experimentally measured material attenuation of $C_6H_5NO_2$ in the visible and near-infrared regions. The transmission spectra of a 9.8 mm thick cuvette filled with $C_6H_5NO_2$ in the visible and near-infrared range are shown in Fig. 3 [34].

A study by Saito et al. [35] proved that the PCF features are strongly affected by the difference in the size of the air holes in the lattice rings. The size of the hole in the first ring directly affects dispersion, including flatness, normal or anomalous dispersion properties, and even zero dispersion wavelength (ZDW) shift. Attenuation is dominated by the rest of the loop. From there, he designed a PCF structure with air holes of diameter $d$ equal to a filling factor of $d_1/\Lambda$ (where $\Lambda$ is the lattice constant) in the first ring (near the core), where $d_1/\Lambda$ varies from 0.3 changes to 0.8 in steps of 0.05. The diameter of the air holes in the remaining lattice rings remains constant as $d$ with a filling factor $d_1/\Lambda = 0.95$. The core diameter depends on $d_1$ and $\Lambda$ is determined by the formula $D_c = 2\Lambda - 1.1d_1$. The simulations use lattice constants $\Lambda = 1.0$ μm, $\Lambda = 1.5$ μm, $\Lambda = 2.0$ μm, and $\Lambda = 2.5$ μm. New features in our design provide minimal attenuation, effective mode area, and chromatic dispersion control for optimal dispersion.

Figure 4 shows the real part characteristic of the wavelength index of refraction of $C_6H_5NO_2$ compared to fused silica. It can be seen that the refractive indices of $C_6H_5NO_2$ and silica glass ($SiO_2$) vary linearly with each other, and the refractive index of $C_6H_5NO_2$ is always greater than that of $SiO_2$. Therefore, light transmitted in $SiO_2$-based PCF with a $C_6H_5NO_2$-core follows the same mechanism of total internal reflection as in conventional optical fibers.

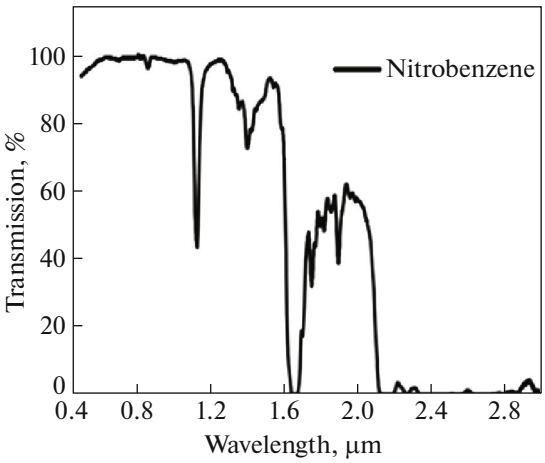


**Fig. 3.** The transmission curves of a 9.8 mm thick cuvette of $C_6H_5NO_2$.

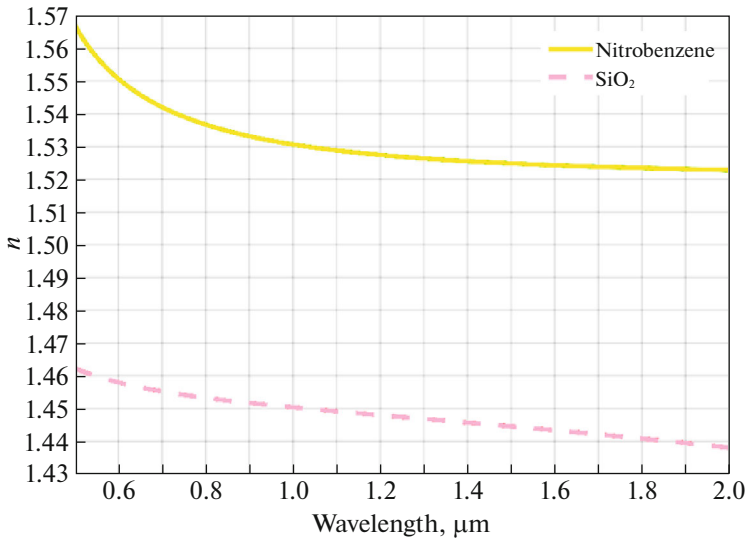


**Fig. 4.** Real parts of the refractive index of $C_6H_5NO_2$ and $SiO_2$.

The real part of the linear refractive index $n$ of $C_6H_5NO_2$ [32] and $SiO_2$ [33] is given by the Sellmeier equation in Eq. (1) as a function of wavelength calculated, with the respective parameters shown in Table 1.

$$n^2(\lambda) = B_0 + \frac{B_1\lambda^2}{\lambda^2 - C_1} + \frac{B_2\lambda^2}{\lambda^2 - C_2} + \frac{B_3\lambda^2}{\lambda^2 - C_3}. \quad (1)$$

Where $\lambda$ is the excitation wavelength in micrometers, $n(\lambda)$ is the wavelength dependent linear refractive index of materials.

Dispersion in an optical fiber includes a waveguide and material dispersion. It is determined according to Eq. (2) [36], where Re $[n_{\text{eff}}]$ is the real part of the effective refractive index of a guided mode and $c$ is the speed of light in a vacuum.

$$D = -\frac{\lambda}{c}\frac{\partial^2 \text{Re}[n_{\text{eff}}]}{\partial\lambda^2}. \quad (2)$$

The units of the nonlinear PCF coefficient are ($W^{-1}$ $km^{-1}$) and are determined by the formula in (Eq. (3)) [36]:

$$\gamma(\lambda) = 2\pi\frac{n_2}{\lambda A_{\text{eff}}}. \quad (3)$$

**Table 1.** Sellmeier's coefficients of the material used

| Nitrobenzene | | Fused silica | |
|---|---|---|---|
| parameters | values | parameters | values |
| $B_0$ | 1 | $B_0$ | 1 |
| $B_1$ | 1.30628 μm$^2$ | $B_1$ | 0.6694226 |
| $B_2$ | 0.00502 μm$^2$ | $B_2$ | 0.4345839 |
| $C_1$ | 0.02268 μm$^4$ | $B_3$ | 0.8716947 |
| $C_2$ | 0.28487 μm$^6$ | $C_1$ | $4.4801 \times 10^{-3}$ μm$^2$ |
| | | $C_2$ | $1.3285 \times 10^{-2}$ μm$^2$ |
| | | $C_3$ | 95.341482 μm$^2$ |

Where $A_{\text{eff}}$ is the effective mode area (an important characteristic of PCF). It is inversely proportional to the nonlinear coefficient and is defined as in Eq. (4) [36]:

$$A_{\text{eff}} = \frac{\left(\int_{-\infty}^{\infty}\int_{-\infty}^{\infty} |E|^2\, dxdy\right)^2}{\int_{-\infty}^{\infty}\int_{-\infty}^{\infty} |E|^4\, dxdy}. \quad (4)$$

Where $E$ is the electric field amplitude.

## OPTIMIZATION OF THE CHARACTERISTIC QUANTITIES OF PCF

Note that optimization algorithms are not used in this article, but better optical properties can be obtained using them. The structural parameters of PCFs can be explained to vary very slightly [37] (for example, the fill factor varies by 0.05 and the lattice constant varies by 0.5 μm, consistent with a "stack-and-draw" manufacturing process of about 50 nm). Moreover, using optimization algorithms during simulation takes a lot of time. Therefore, a simpler method based on the optimization of dispersion properties was applied.

The chromatic dispersion strongly depends on wavelength, the value of the filling factor $d_1/\Lambda$, and the lattice constant $\Lambda$, as shown in Fig. 5. It can be clearly observed that the $C_6H_5NO_2$-PCFs exhibit both all-normal and anomalous dispersions with one or two ZDWs for smaller core PCFs, $\Lambda = 1.0$ μm (Fig. 5a). Furthermore, as $d_1/\Lambda$ increases, the right edge increases and the left edge shrinks. When $d_1/\Lambda$ is less than 0.4, the curve dispersion lies in one ZDW anomalous dispersion region and shifts towards two ZDW anomalous dispersion regions with increasing values of $d_1/\Lambda$ (from 0.7 to 0.8). Otherwise, the dispersion curve falls within the all-normal dispersion region, and increasing the value of the filling factor $d_1/\Lambda$ (0.4 to 0.65) brings the all-normal dispersion closer to the zero dispersion curve, which should be beneficial for SC generation. The interaction between waveguide dispersion and material dispersion can be responsible for small-core dispersion diversity. At smaller $d_1/\Lambda$, material dispersion dominates, while at larger $d_1/\Lambda$ waveguide effects play a major role.

For $\Lambda > 1.0$ μm ($\Lambda = 1.5$, 2.0, 2.5 μm (Figs. 5b, 5c, 5d)), we observed significant changes in the nature of the dispersion profile of PCFs with larger cores, suggesting that the anomalous dispersion regime with one ZDW dominant completely in the investigated wavelength range. For a given value of $d_1/\Lambda$, increasing the lattice constant shifts the ZDW to longer wavelengths. For $\Lambda = 1.5$, 2.0, and 2.5 μm, the PCF exhibits an anomalous dispersion region that shifts from the ZDW to the short wavelength region as $d_1/\Lambda$ increases. The flattest, closest to zero-dispersion curve has $d_1/\Lambda = 0.3$ and $\Lambda = 2.0$ μm. The above analysis and simulation results show that by carefully tuning the air hole diameter $d_1$ of the first ring of the PCF structure, it seems that the desired dispersion properties of the structure can be easily obtained.

Small and flat dispersion over a wide wavelength range is always favorable for SC generation. In addition, pump wavelength, pulse duration, peak power, and fiber length are also determinants of broadband SC generation [38]. Based on the preliminary analysis of the dispersion, we propose two PCFs with

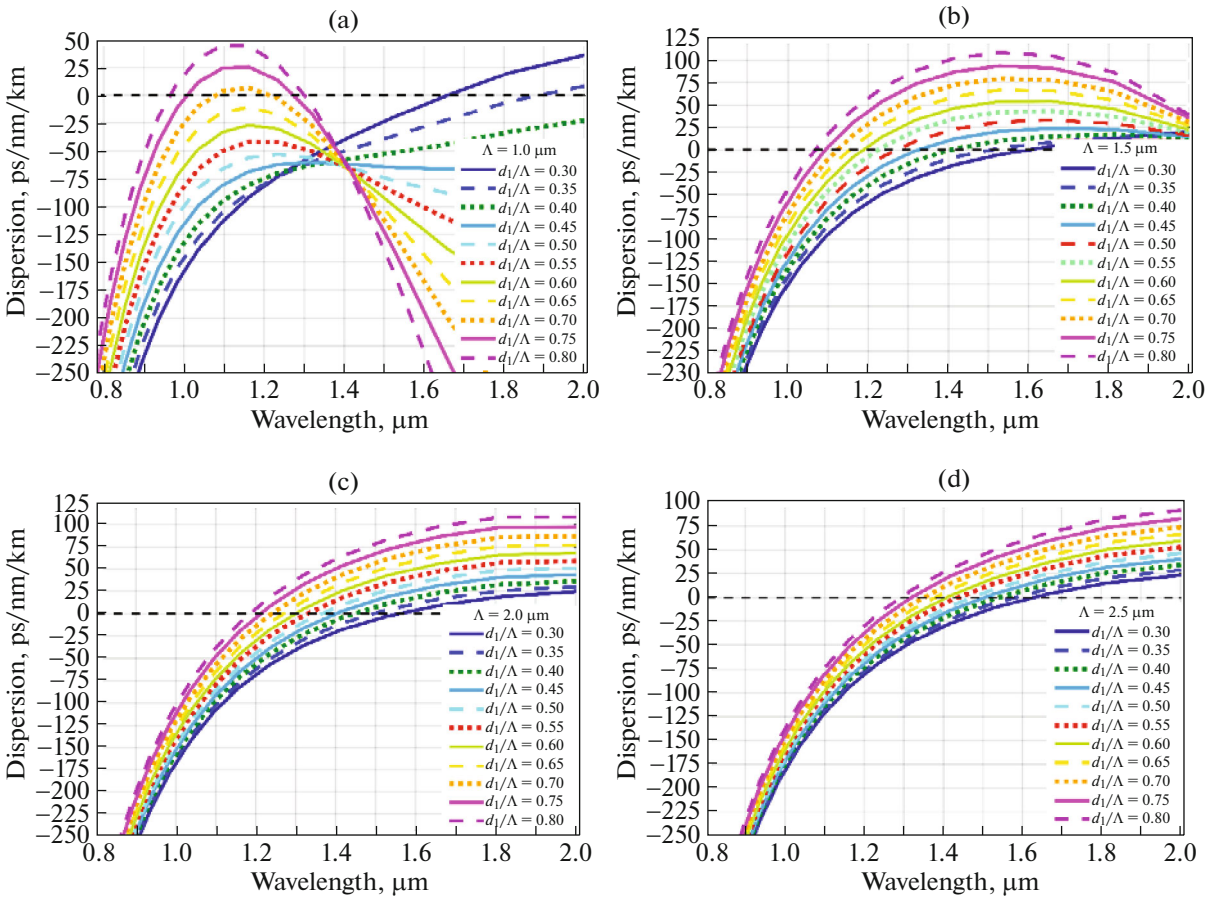


**Fig. 5.** The plot of the D-parameter against the wavelength for PCFs with different Λ values equal (a) 1.0 μm, (b) 1.5 μm, (c) 2.0 μm, and (d) 2.5 μm. $d_1/\Lambda$ varies from 0.3 to 0.8.

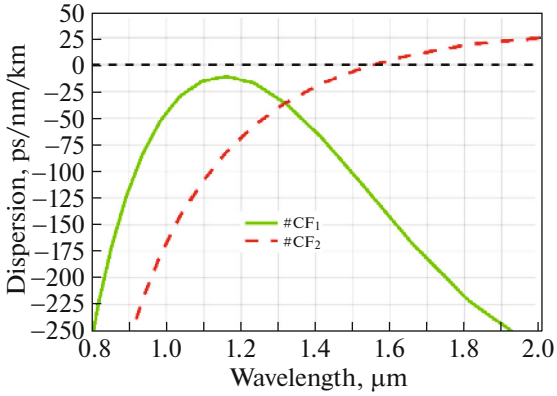


**Fig. 6.** The chromatic dispersion characteristics of the fundamental mode for #$CF_1$ and #$CF_2$ fibers.

appropriate dispersion and examine SC generations named #$CF_1$ and #$CF_2$ in detail. Dispersion appears flatter and closer to zero dispersion compared to other fibers. Based on this, we selected two optimal fibers for SCG, namely #$CF_1$ ($d_1/\Lambda = 0.65$; $\Lambda = 1.0$ μm) and #$CF_2$ ($d_1/\Lambda = 0.3$; $\Lambda = 2.0$ μm). Figure 6 shows the dispersion characteristics of the proposed fiber. The #$CF_1$ fiber operates in an all-normal dispersion range and has a maximum dispersion value of $-10.86$ ps nm$^{-1}$ km$^{-1}$ at a wavelength of 1.161 μm. SC generation with an all-normal dispersion range PCF has the great advantage of making the output pulse coherent, very stable, and flat, which makes any work effort possible. We choose the pump wavelength

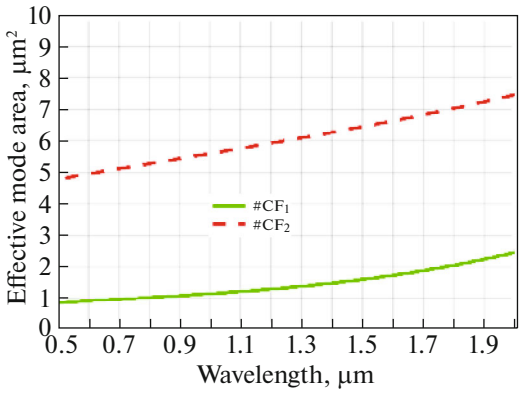


**Fig. 7.** The effective mode area of the fundamental mode for #$CF_1$ and #$CF_2$ fibers.

at 1.3 μm for the #$CF_1$ fiber because this value is close to the wavelength value at the maximum point of the dispersion curve. This extends the spectrum of the fiber. On the other hand, the #$CF_2$ fiber has anomalous dispersion and a zero dispersion wavelength (ZDW) at 1.547 μm. Therefore, we chose a pump wavelength of 1.56 μm for the #$CF_2$ fiber (the pump wavelength chosen here satisfies the condition of having a larger value and being close to the zero-dispersion wavelength). The dispersions of #$CF_1$ and #$CF_2$ fibers at the pump wavelength are –31.866 ps $nm^{-1}$ $km^{-1}$ and 0.229 ps $nm^{-1}$ $km^{-1}$, respectively.

As the ultra-short pulses propagate along the fiber, they interact with nonlinear optical media and generate new frequencies through various nonlinear effects, broadening the SC spectrum. Therefore, the nonlinear properties of optical fibers play an important role in improving SC efficiency. Due to the large refractive index contrast between the core and the cladding, the light can be better confined in the core of his PCF, improving the nonlinear coefficients as expected. Figure 7 shows the effective mode area of the two proposed fibers. The effective mode area value increases with increasing wavelength. This value for fibers #$CF_1$ and #$CF_2$, calculated at the pump wavelength, is 1.388 $\mu m^2$ and 6.565 $\mu m^2$ respectively, which are relatively small compared to these values shown in Table 2. The nonlinear coefficient is inversely proportional to the effective modal area according to Eq. (3). Therefore, it tends to decrease linearly with increasing wavelength, as shown in Fig. 8. The nonlinearity of fiber #$CF_1$ is always larger than that of #$CF_2$, and at the pump wavelength the nonlinearity value of #$CF_1$ is 2220 $W^{-1}$ $km^{-1}$, for #$CF_2$ 469 $W^{-1}$ $km^{-1}$. Figure 9 shows the fundamental mode attenuation characteristics of #$CF_1$ and #$CF_2$ fibers. The attenuation of #$CF_2$ fiber is the smallest, which is almost the same as the horizontal axis. The attenuation value at 1.3 pump wavelength for #$CF_1$ fiber is 30.2 dB/m. Very low attenuation is an advantage of our model compared to previous studies.

**Table 2.** The structure parameters and the characteristic quantities of proposed PCFs at the pump wavelength in comparison with some previous work of liquid-filled PCFs

| # | Pump wavelength, μm | $D$, ps/(nm km) | $A_{eff}$, $\mu m^2$ | γ, $km^{-1}$ $W^{-1}$ | Attenuation, dB/m | Regime |
|---|---|---|---|---|---|---|
| #$CF_1$ | 1.3 | –31.866 | 1.388 | 2220 | 30.2 | All-normal |
| #$CF_2$ | 1.56 | 0.229 | 6.565 | 469 | 0 | Anomalous |
| $CCl_4$ [21] | 1.03 | –85 | 42.2 | 22.1 | – | All-normal |
| $C_7H_8$ [12] | 1.55 | –7.784 | 7.79 | 1200 | 40 | All-normal |
| $C_7H_8$ [12] | 1.55 | –1.19 | 78.9 | – | 120 | Anomalous |
| $C_7H_8$ [26] | 1.03 | –150...–5 | 73.2 | 130 | – | All-normal |

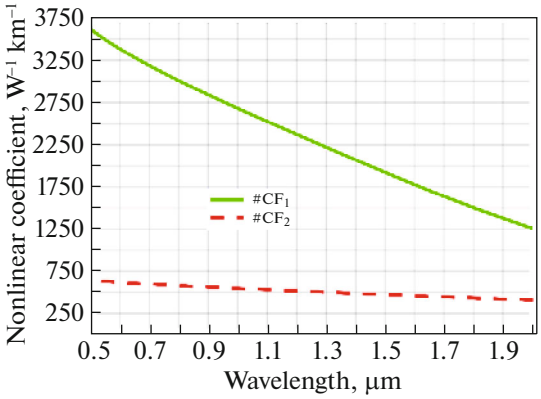


**Fig. 8.** The nonlinear coefficient of the fundamental mode for #$CF_1$ and #$CF_2$ fibers.

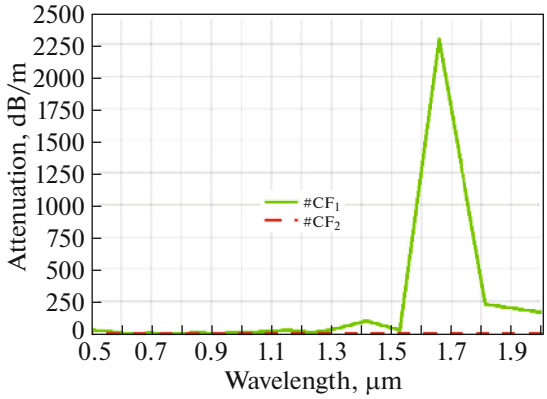


**Fig. 9.** The attenuation of the fundamental mode for #$CF_1$ and #$CF_2$ fiber.

## SUPERCONTINUUM GENERATION IN PROPOSED FIBER

Higher-order dispersion shows a significant effect as the center wavelength of the input pulse approaches ZDW and is calculated by the broadening coefficients of the Taylor series around the center wavelength $\omega_0$, the expansion of the propagation constant ($\beta$) can be obtained by [36]

$$\beta(\omega) = \beta(\omega_0) + \beta_1(\omega_0)(\omega - \omega_0) + \frac{1}{2!}\beta_2(\omega_0)(\omega - \omega_0)^2 + \ldots \quad (5)$$

The $n_{th}$ order dispersion term can then be calculated by taking the derivative of $\beta$ with respect to the angular frequency $\omega$ [27]

$$\beta_n = \left.\frac{d^n\beta}{d\omega^n}\right|_{\omega=\omega_0}. \quad (6)$$

Table 3 shows the higher-order dispersion at the pump pulse frequency in numerical modeling.

The nonlinear propagation process of the pump pulse in the PCF can be described by the Schrödinger equation (GNLSE) using the symmetric split-step Fourier transform method [36], which is given by the formula:

$$\partial_z\tilde{A} - i\tilde{\beta}(\omega)\tilde{A} - \frac{\tilde{\alpha}(\omega)}{2}\tilde{A} = i\gamma\left(1 + \frac{\omega - \omega_0}{\omega_0}\right)\tilde{A}F\left[\int_{-\infty}^{\infty} R(T')|A|^2(T - T')dT'\right]. \quad (7)$$

Where $\tilde{A}(\omega)$ is Fourier transform of the amplitude of the pulse $A(t)$, and $R(T')$ is the Raman response function. The nonlinear material response function $R(T)$ is described by a function that describes two

**Table 3.** The SC bandwidth of proposed PCFs in comparison with other silica-based PCF infiltration with liquid

| # | References | Peak power, W | Pump wavelength, μm | Fiber length, cm | SC spectral range, μm | Regime |
|---|---|---|---|---|---|---|
| #$CF_1$ | This work | 133 | 1.3 | 1 | 0.72–1.722 | All-normal |
| #$CF_2$ | This work | 273 | 1.56 | 15 | 0.795–3.748 | Anomalous |
| $CCl_4$ | [21] | 62500 | 1.03 | 20 | 0.85–1.25 | All-normal |
| $CHCl_3$ | [22] | 2500 | 1.03 | 10 | 0.6–1.26 | All-normal |
| | | 2000 | 1.03 | 10 | 0.6–1.4 | Anomalous |
| $C_6H_5NO_2$ | [15] | 5550 | 1.56 | 5.0 | 0.8—2.1 | All-normal |
| | | 660 | 1.56 | 5.0 | 1.3–2.3 | Anomalous |
| $C_6H_6$ | [23] | 55000 | 1.56 | 1.0 | 0.7–2.0 | All-normal |
| | | 37000 | 1.56 | 1.0 | 0.6–3.5 | Anomalous |
| $C_2Cl_4$ | [16] | 16670 | 1.56 | 5.0 | 0.8—2.0 | All-normal |
| | | 16670 | 1.56 | 10 | 1.0–2.0 | Anomalous |
| | | 20830 | 1.03 | 10 | 0.7–2.4 | Anomalous |
| $C_2H_4Br_2$ | [25] | 12500 | 1.03 | 10 | 0.64–1.7 | All-normal |
| | [25] | 750 | 1.03 | 15 | 0.7–2.4 | Anomalous |
| $C_7H_8$ | [12] | 7140 | 1.55 | 10 | 1.1–1.75 | All-normal |
| | [12] | 6670 | 1.55 | 10 | 1.0–1.75 | Anomalous |
| $C_7H_8$ | [26] | 25000 | 1.03 | 10 | 0.95–1.1 | All-normal |
| $C_7H_8$ | [29] | 450 | 1.064 | 1 | 0.642–1.592 | All-normal |
| | [29] | 550 | 1.55 | 10 | 0.911–2.496 | Anomalous |

damped harmonic oscillators with the main contributions from the electronically coupled and core parts, assuming that the electronic factor is the instantaneous mechanism [36].

$$R(T) = (1 - f_R)\,\delta(T) + f_R h_R(T), \tag{8}$$

where $\delta(T)$ is the Dirac delta function and $h_R(T)$ is the delay response. The delay characteristics of the nonlinear response is comparable to the Raman-induced frequency shift, i.e. energy is transferred to larger wavelengths which are accompanied by a redshift. Therefore, we can fine that fractional contribution of delayed Raman to the total nonlinear response can be found after normalizing $h_R(T)$: [36]

$$h_R(T) = \frac{\tau_1^2 + \tau_2^2}{\tau_1^2 \tau_2^2} \exp\left(\frac{-T}{\tau_1}\right) \sin\left(\frac{T}{\tau_2}\right) \Theta(T), \tag{9}$$

where $\Theta(T)$ is the Heaviside step function.

A Gaussian impulse is assumed to act as the input impulse, expressed with axial propagation $z = 0$ as follows [39]:

$$A_1(z = 0, t) = \sqrt{P_0} \exp\left(-\frac{t^2}{2t_0^2}\right)$$
$$A_2(z = 0, t) = 0, \tag{10}$$

where $A$ represents the electric field envelope of the optical pulse and $P_0$ is the peak power. The parameters $t$ and $t_0$ are known as the input pulse delay time and pulse duration.

For #$CF_1$ and #$CF_2$ fibers various nonlinear phenomena occurring during SC simulations are common for both all-normal and anomalous dispersion. Using a low peak power pump pulse to obtain a broad SC spectrum in these simulations has two distinct advantages. First, the refractive index of $C_6H_5NO_2$ is many times higher than that of fused silica. Second, the proposed two fibers are highly nonlinear due to

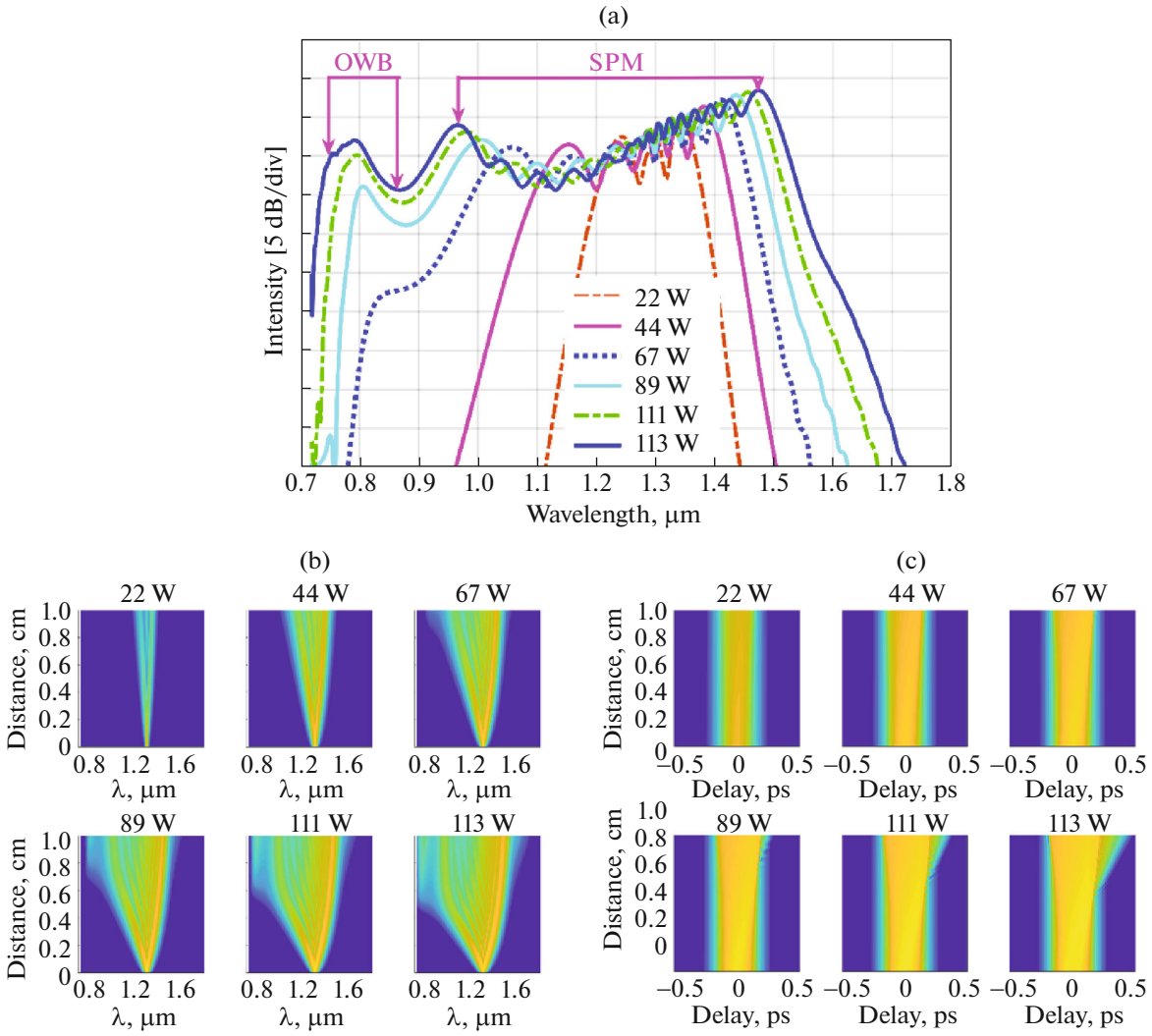


**Fig. 10.** For #$CF_1$ fiber: (a) the output spectra for various input pulse energies when using pump pulses with 1.3 μm pump wavelength and 90 fs duration, (b) the pulse evolution of the SC along with fiber, and (c) the temporal profile at various propagation length.

their small effective areas. In particular, #$CF_1$ fiber produces a broad and flat SC spectrum associated with all-normal dispersion properties, while #$CF_2$ produces a very broad and noisy SC spectrum in the anomalous dispersion region. The SC generation of #$CF_1$ fiber was pumped at 1.3 μm, with a pulse duration of 90 fs and peak power varying from 22 to 133 W. The pulse transmission length of #$CF_1$ fiber is 1 cm. A #$CF_2$ fiber with a ZDW of 1.547 μm and SC generation with peak powers ranging from 9 to 273 W at a propagation length of 15 cm, a pump wavelength of 1.56 μm and a pulse duration of 110 fs was analyzed.

Figure 10 shows the temporal and spectral evolution of the pulse over a propagation distance of 1 cm using different peak powers in the #$CF_1$ fiber. Since #$CF_1$ has pump pulses that operate with all-normal dispersion, so the SC generation process is dominated by two main effects, the SC generation process is dominated by two main effects, namely SPM and OWB. Looking at Fig. 10a, we can see that as the peak power increases, so does the spectral width. For low peak power pump fibers of 22 and 44 W, SPM makes the greatest contribution to spectral broadening. This results in a finitely conserved spectrum and a spectrum composed of many peaks, with the extreme peaks having the greatest intensity. When the peak power is greater than 44 W, the SC spectrum is determined by the SPM in the early stages of propagation and the resulting spectrum is asymmetric for short wavelengths due to the nonlinear dispersion effect of dispersion. Subsequently, the emergence of OWB generated by four-wave mixing (FWM) was the dominant

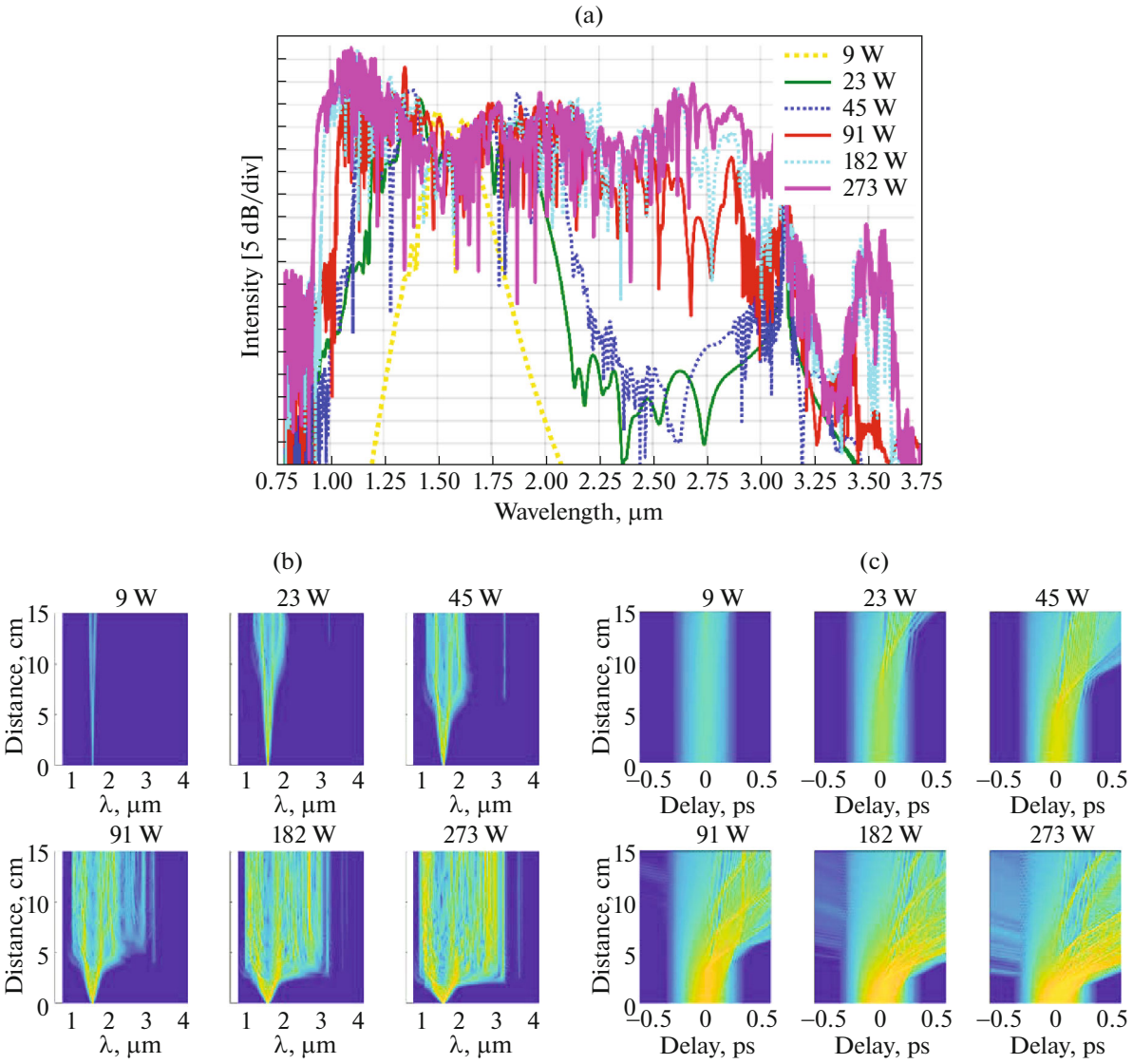


**Fig. 11.** For #$CF_2$ fiber: (a) the output spectra for various input pulse energies when using pump pulses with 1.56 μm pump wavelength and 110 fs duration, (b) the pulse evolution of the SC along the fiber, and (c) the temporal profile at various propagation length.

effect in spectral broadening in these cases. OWB begins to appear at 67 W peak power at 0.86 μm and helps the spectrum expand rapidly as peak power continues to increase, with OWB appearing at shorter wavelengths. At a peak power of 133 W, the spectrum extends from 0.72 to 1.722 μm with a relative power range of 5 dB. Figure 10c shows the temporal structure at different positions in the propagation length according to the spectrum growing along the #$CF_1$ fiber. In general, the higher the input peak power, the faster the time delay between different frequencies and the shorter the propagation. Considered in each case, these values increase with increasing distance due to different group velocity components.

In this section, we investigate how the anomalous dispersion affects SC generation in a 1.56 μm pumped #$CF_2$ fiber (Fig. 11). Since the #$CF_2$ fiber has a pump wavelength within the anomalous dispersion range, soliton dynamics, such as soliton fission (SF) and soliton self-frequency shift (SSFS), play an important role in spectral broadening. So its SC spectrum is much broader than the #$CF_1$ fiber, and unfortunately its noise spectrum is larger. Figure 11 shows the spectral evolution at different peak powers. At a peak power of 9 W, the SPM plays a major role in spectral broadening, so the resulting spectrum is smaller in this case. Beyond a peak power of 9 W, soliton fission begins to appear, broadening the spectrum. As peak power increases, spectral width increases. However, when the peak power is 273 W, the

spectral width is almost the same as when the peak power is 182 W. This is explained by factors such as high dispersion slope in the short wavelength range, low nonlinear coefficient and high loss in the long wavelength range. When the peak power equals 273 W, the spectral bandwidth expands from 0.795 to 3.748 μm with a dynamic range of 5 dB.

The SC bandwidth of the PCFs in our study should be compared to highly nonlinear liquid-filled fibers. As can be seen from Table 4, the $\#CF_1$ structure can achieve the same or higher bandwidth than previous releases but uses much less peak power. The SC produced by $\#CF_2$ is the widest SC reported when the fiber is pumped in an anomalous dispersion regime and is also the only fiber for which the lowest peak power should be used. The above results show the high potential of the proposed PCFs for a wide SC generation system with low peak power.

## CONCLUSIONS

The $C_6H_5NO_2$-filled PCF with diverse dispersion was designed by adjusting the diameters $d_1$ and $d$ of the first ring near the core and others in the mantle of the PCF to simultaneously optimize the characteristic quantities of the PCF. Two fibers with flat dispersion, high nonlinearity, and low loss are included for a detailed study of the SC generation process. A $\#CF_1$ fiber with lattice constant $\Lambda = 1.0$ μm and filling factor $d_1/\Lambda = 0.65$ has an all-normal dispersion regime and produces a flat and wide SC by the SPM effect followed by OWB. A wide spectral range of 0.72 to 1.722 μm is easily achieved with a low peak input power of 133 W at the 1.3 μm pump wavelength. A $\#CF_2$ fiber ($\Lambda = 2.0$ μm and $d_1/\Lambda = 0.3$) produces a wide SC with a spectral bandwidth of 2.953 μm within 5 dB. Soliton dynamics contribute significantly to the SC process as the fiber is pumped in an anomalous dispersion mode with a pump wavelength of 1.56 μm and a low peak power of 273 W.

The above simulation analysis results show that the nonlinear effects that play an important role in SC generation are often dominated by the dispersion and nonlinear properties of the PCF. The high nonlinearity and reasonable structural changes of $C_6H_5NO_2$ are also the main factors that enable PCF to produce a broader spectrum with low input peak power and short transmission distance. It achieves broader SC spectra in all normal and anomalous dispersions compared to other liquid-filled PCFs [12, 15, 16, 21–23, 25, 26, 29]. The development of PCF could become a new fiber layer for next-generation broadband sources.

## CONFLICT OF INTEREST

The authors declare that they have no conflicts of interest.

## REFERENCES

1. Dudley, J.M., Genty, G., and Coen, S., Supercontinuum generation in photonic crystal fiber, *Rev. Mod. Phys.*, 2006, vol. 78, pp. 1135–1184. https://doi.org/10.1103/RevModPhys.78.1135
2. Pires, M., Baudisch, M., Sanchez, D., Hemmer, M., and Biegert, J., Ultrashort pulse generation in the mid-IR, *Progr. Quant. Electron.*, 2015, vol. 43, pp. 1–30. https://doi.org/10.1016/j.pquantelec.2015.07.001
3. Smirnov, S.V., Ania-Castanon, J.D., Ellingham, T.J., Kobtsev, S.M., Kukarin, S., and Turitsyn, S.K., Optical spectral broadening and supercontinuum generation in telecom applications, *Opt. Fiber Technol.*, 2006, vol. 12, no. 2, pp. 122–147. https://doi.org/10.1016/j.yofte.2005.07.004
4. Chu, V.L., Mai, V.L., and Ho, Q.Q., Reduction thermo-optic nonlinearity in the Raman laser generating Stokes and anti -Stokes waves pumped by CW Gaussian beam, *Commun. Phys.*, 2008, vol. 18, no. 4, pp. 255–262.
5. Chu, V.L., Mai, V.L., Dinh, X.K., Vu, N.S., Nguyen, T.T.T., and Ho, Q.Q., Nonlinear characteristics of the pulse-pumped anti-Stokes laser, *Commun. Phys.*, 2008, vol. 18, no. 2, pp. 119–128.
6. Chu, V.L. and Dinh, X.K., Competition between Stokes and anti-Stokes waves in CW-Raman fiber laser, *Commun. Phys.*, 2007, vol. 17, no. 4, pp. 227–233.
7. Heidt, A.M., Hartung, A., Bosman, G.W., Krok, P., Rohwer, E.G., Schwoerer, H., and Bartelt, H., Coherent octave spanning near-infrared and visible supercontinuum generation in all-normal dispersion photonic crystal fibers, *Optics Express*, 2011, vol. 19, pp. 3775–3787. https://doi.org/10.1364/OE.19.003775

8. Medjouri, A., Abed, D., Ziane, O., and Simohamed, L.M., Design and optimization of $As_2S_5$ chalcogenide channel waveguide for coherent mid-infrared supercontinuum generation, *Optik*, 2018, vol. 154, pp. 811–820. https://doi.org/10.1016/j.ijleo.2017.10.135
9. Liu, H.H., Yu, Y., Song, W., Jiang, Q., and Pang, F.F., Recent development of flat supercontinuum generation in specialty optical fibers, *Opto-Electron. Adv.*, 2019, vol. 2, no. 2, p. 1800201.
10. Jia, Z.X., Yao, C.F., Jia, S.J., Wang, F., Wang, S.B., Z. P. Zhao, Z.P., Liao, M.S., Qin, G.S., Hu, L.L., Ohishi, Y., and Qin, W.P., Supercontinuum generation covering the entire 0.4–5 μm transmission window in a tapered ultra-high numerical aperture all-solid fluorotellurite fiber, *Laser Phys. Lett.*, 2018, vol. 15, no. 2, p. 025102. https://doi.org/10.1088/1612-202X/aa8bc2
11. Dai, S., Wang, Y., Peng, X., Zhang, P, Wang, X. and Xu, Y., A Review of mid-infrared supercontinuum generation in ghalcogenide glass fibers, *Appl. Sci.*, 2018, vol. 8, no. 5, p. 7071. https://doi.org/10.3390/app8050707
12. Chu, V.L., Anuszkiewicz, A., Ramaniuk, A., Kasztelanic, R., Dinh, X.K., Cao, L.V., Trippenbach, M., and Buczyński, R., Supercontinuum generation in photonic crystal fibres with core filled with toluene, *J. Opt.*, 2017, vol. 19, no. 12, p. 125604. https://doi.org/10.1088/2040-8986/aa96bc
13. Chu, V.L., Nguyen, T.T., Hoang, T.D., Le, T.B.T., Vo, T.M.N., Dang, V.T., Le, C.T., Ho, D.Q., and Doan, Q.K., Comparison of supercontinuum spectrum generating by hollow core PCFs filled with nitrobenzene with different lattice types, *Opt. Quant. Electron.*, 2022, vol. 54, p. 300. https://doi.org/10.1007/s11082-022-03667-y
14. Dang, N.T., Nguyen, M.L., Dang, L.C., Nguyen, T.T., Tran, Q.V., Dinh, X.K., and Chu, V.L., Photonic crystal fiber with core infiltrated carbon tetrachloride for nonlinear effects generation, *Advances in Applied and Engineering Physics – CAEP V*, 2018, pp. 200–205.
15. Chu, V.L., Hoang, V.T., Cao, L.V., Borzycki, K., Dinh, X.K., Tran, Q.V., Trippenbach, M., Buczynski, R., and Pniewski, J., Supercontinuum generation in photonic crystal fibers infiltrated with nitrobenzene, *Laser Phys.*, 2020, vol. 30, no. 3, p. 035105. https://doi.org/10.1088/1555-6611/ab6f09
16. Le, V.H., Hoang, V.T., Nguyen, T.H., Cao, L.V., Buczyński, R., and Kasztelanic, R., Supercontinuum generation in photonic crystal fibers infiltrated with tetrachloroethylene, *Opt. Quant. Electron.*, 2021, vol. 53, p. 187. https://doi.org/10.1007/s11082-022-03667-y
17. Churin, D., Nguyen, T.N., Kieu, K., Norwood, R.A., and Peyghambarian, N., Mid-IR supercontinuum generation in an integrated liquid-core optical fiber filled with CS2, *Opt. Mater. Express*, 2013, vol. 3, pp. 1358–1364. https://doi.org/10.1364/OME.3.001358
18. Junaid, S., Bierlich, J., Hartung, A., Meyer, T., Chemnitz, M., and Schmidt, M.A., Supercontinuum generation in a carbon disulfide core microstructured optical fiber, *Opt. Express,* 2021, vol. 29, no. 13, pp. 19891–19902. https://doi.org/10.1364/OE.426313
19. Ho, D.Q., Pniewski, J., Le, V.H., Ramaniuk, A., Cao, L.V., Borzycki, K., Dinh, X.K., Klimczak, M., and Buczynski, R., Optimization of optical properties of photonic crystal fibers infiltrated with carbon tetrachloride for supercontinuum generation with subnanojoule femtosecond pulses, *Appl. Opt.*, 2018, vol. 57, no. 14, pp. 3738–3746. https://doi.org/10.1364/AO.57.003738
20. Hoang, V.T., Kasztelanic, R., Stepniewski, G., Dinh, X.K., Cao, L.V., Trippenbach, M., Klimczak, M., Buczynski, R. and Pniewski, J., Femtosecond supercontinuum generation around 1560 nm in hollow-core photonic crystal fibers filled with carbon tetrachloride, *Appl. Opt.*, 2020, vol. 59, no. 12, pp. 3720–3725. https://doi.org/10.1364/AO.385003
21. Hoang, V.T., Kasztelanic, R., Filipkowski, A., Stepniewski, G., Pysz, D., Klimczak, M., Ertman, S., Cao, L.V., Wolin'ski, T.R., Trippenbach, M., Dinh, X.K., S'mietana, M., and Buczynski, R., Supercontinuum generation in an all-normal dispersion large core photonic crystal fiber infiltrated with carbon tetrachloride, *Opt. Mater. Express*, 2019, vol. 9, no. 5, pp. 2264–2278. https://doi.org/10.1364/OME.9.002264
22. Chu, V.L., Hoang, V.T., Cao, L.V., Borzycki, K., Dinh, X.K., Tran, Q.V., Trippenbach, M., Buczynski, R., and Pniewski, J., Optimization of optical properties of photonic crystal fibers infiltrated with chloroform for supercontinuum generation, *Laser Phys.*, 2019, vol. 29, no. 7, p. 075107. https://doi.org/10.1088/1555-6611/ab2115
23. Chu, V.L., Hoang, V.T., Cao, L.V., Borzycki, K., Dinh, X.K., Tran, Q.V., Trippenbach, M., Buczyński, R., and Pniewski, J., Supercontinuum generation in benzene-filled hollow-core fibers, *Opt. Eng.*, 2021, vol. 60, no. 11, p. 116109. https://doi.org/10.1117/1.OE.60.11.116109

24. Chu, V.L., Le, V.H., Dang, N.N., Vo, T.M.N., Ho, D.Q., Hoang, V.T., Nguyen, T.T., and Chu, V.B., Modelling of lead-bismuth gallate glass ultra-flatted normal dispersion photonic crystal fiber infiltrated with tetrachloroethylene for high coherence mid-infrared supercontinuum generation. *Laser Physics*, 2022, vol. 32, p. 055102. https://doi.org/10.1088/1555-6611/ac599b

25. Le, V.H., Hoang, V.T., Ho, D.Q., Nguyen, T.H., Vo, T.M.N., Klimxzak, M., Buczynski, R., and Kasztelanic, R., Silica-based photonic crystal fiber infiltrated with 1,2-dibromoethane for supercontinuum generation, *Appl. Opt.*, 2021, vol. 60, no. 24, pp. 7268–7278. https://doi.org/10.1364/AO.430843

26. Hoang, V.T., Kasztelanic, R., Anuszkiewicz, A., Stepniewski, G., Filipkowski, A., Ertman, S., Pysz, D., Wolinski, T., Dinh, X.K., Klimczak, M., and Buczynski, R., All-normal dispersion supercontinuum generation in photonic crystal fibers with large hollow cores infiltrated with toluene, *Opt. Mater. Express*, 2018, vol. 8, no. 11, pp. 3568–3582. https://doi.org/10.1364/OME.8.003568

27. Raei, R., Ebnali-Heidari, M., and Saghaei, H., Supercontinuum generation in organic liquid-liquid core-cladding photonic crystal fiber in visible and near-infrared regions, *J. Opt. Soc. Am. B*, 2018, vol. 35, no. 2, pp. 323–330. https://doi.org/10.1364/JOSAB.35.000323

28. Maji, P.S. and Chaudhuri, P.R., Supercontinuum generation in ultra-flat near zero dispersion PCF with selective liquid infiltration, *Optik*, 2014, vol. 125, p. 5986. https://doi.org/10.1016/j.ijleo.2014.07.026

29. Nguyen, T.T., Hoang, T.D., Le, T.B.T., Dang, V.T., and Chu, V.L., Optimization of optical properties of toluene-core photonic crystal fibers with circle lattice for supercontinuum generation, *J. Opt.*, 2022, vol. 51, pp. 678–688. https://doi.org/10.1007/s12596-021-00802-y

30. Mode Solution. Lumerical Solutions, Inc. www.lumerical.com/tcad-products/mode

31. Vieweg, M., Gissibl, T., Pricking, S., Kuhlmey, B.T., Wu, D.C., Eggleton, B.J., and Giessen, H., Ultrafast nonlinear optofluidics in selectively liquid-filled photonic crystal fibers, *Opt. Express*, 2010, vol. 18, pp. 25232–25240. https://doi.org/10.1364/OE.18.025232

32. Kedenburg, S., Vieweg, M., Gissibl, T., and Giessen. H., Linear refractive index and absorption measurements of nonlinear optical liquids in the visible and near-infrared spectral region, *Opt. Mater. Express*, 2012, vol. 2, pp. 1588–1611. https://doi.org/10.1364/OME.2.001588

33. Tan, C.Z., Determination of refractive index of silica glass for infrared wavelengths by IR spectroscopy, *J. Non-Cryst. Solids*, 1998, vol. 223, pp. 158–163. https://doi.org/10.1016/S0022-3093(97)00438-9

34. Zhang, R., Teipel, J., and Giessen, H., Theoretical design of a liquid-core photonic crystal fiber for supercontinuum generation, *Opt. Express*, 2006, vol. 14, no. 15, pp. 6800–6812. https://doi.org/10.1364/OE.14.006800

35. Saitoh, K., Koshiba, M., Hasegawa, T., and Sasaoka, E., Chromatic dispersion control in photonic crystal fibers: Application to ultra-flattened dispersion, *Opt. Express*, 2003, vol. 11, no. 8, pp. 843–852. https://doi.org/10.1364/OE.11.000843

36. Agrawal, G.P., *Nonlinear Fiber Optics*, Berlin: Springer, 2000. https://doi.org/10.1007/3-540-46629-0_9

37. Pysz, D., Kujawa, I., Stępień, R., Klimczak, M., Filipkowski, A., Franczyk, M., Kociszewski, L., Buźniak, J., Haraśny, K., and Buczyński, R., Stack and draw fabrication of soft glass microstructured fiber optics, *Bull. Polish Acad. Sci., Tech. Sci.*, 2014, vol. 62, no. 4, pp. 667–682.

38. Corwin, K.L., Newbury, N.R., Dudley, J.M., Coen, S., Diddams, S.A., Weber, K., and Windeler, R.S., Fundamental Noise Limitations to Supercontinuum Generation in Microstructure Fiber, *Phys. Rev. Lett.*, 2003, vol. 90, p. 113904. https://doi.org/10.1103/PhysRevLett.90.113904

39. Koohi-Kamalia, K., Ebnali-Heidarib, M. and Moravvej-Farshic, M.K., Designing a dual-core photonic crystal fiber coupler by means of microfluidic infiltration, *Int. J. Opt. Photon.*, 2012, vol. 6, no. 2. pp. 83–96.